Chapter 8
Wave climate and energy dissipation near Santa Cruz Island, California

Nathan Burley [a*] and Robyn Suddeth [b]

[a]Civil & Environmental Engineering
[b]Graduate Group in Hydrologic Sciences
University of California, Davis, CA 95616
*nburley@ucdavis.edu

Abstract

Offshore wave characteristics and nearshore transformation processes determine wave energy dissipation along coastlines. Wave impacts are a primary driver of coastal geomorphology, factoring into rates of cliff retreat and shoreline response. In this study the wave regime near Santa Cruz Island, California is presented and wave energy dissipation is calculated for different locations around the island. A model is used to estimate increased nearshore wave height and to verify breaking or reflecting wave conditions. Generalized refraction coefficients (K_R) on W-NW swell and 10 m bathymetry is calculated. Energy dissipated on coastlines is modeled through reflected waves (in deep water) and breaking waves (in shallow water). The highest energy dissipation rates are on the northwestern corner of the island, confirming the significance of refraction effects. Southern shorelines experience lower energy dissipation due to high K_R values, offshore sheltering by Santa Rosa Island, and a weaker southern swell. The results of this analysis are used in Chapter 9 to characterize patterns and rates and of coastal erosion of Santa Cruz Island.

Introduction

Wave energy and dissipation rates on coastlines are highly variable. Incoming wave characteristics, shoreline topography and bathymetry drive dissipation processes. Local wave regime is set up by long period oceanic swells and subsequent wave transformations in the nearshore environment. The effect of nearshore wave transformation generally reduces total wave energy and creates unique waveforms. Waves are transformed into breaking or reflecting waves, depending on their characteristics and nearshore bathymetry. Each wave type has a signature wave pressure that is felt by the shoreline as the wave breaks or reflects. Offshore wave energy is traditionally calculated per wavelength per unit crest width (Sorensen, 1978) or as an energy flux (Dean and Dalrymple, 1991), while nearshore wave energy is calculated as a breaking or impulse pressure per unit coastline (USACE, 1984).

Offshore wave energy or flux is useful for obtaining a general understanding of regional conditions, but knowledge of shoreline impacts requires more detail. Significant factors

determining shoreline wave energy dissipation include: swell direction, refraction and diffraction, coastal currents, local wave conditions and seasonality. Swell direction interacts with bathymetry and shoreline geometry to create refraction and diffraction patterns that generally reduce incident wave energy. Local conditions and coastal currents can also interfere with swell energy or become the dominant energy source for a shoreline orientation. Seasonality affects the frequency, size and timing of wave events.

This case study applies wave climate information from Xu and Noble (2009) and bathymetry data from United States Geological Survey (USGS) to provide a description of incident wave pressures upon the Santa Cruz Island coastline. This work is extended in Chapter 9 to estimate cliff retreat and shoreline response to give an overall picture of the coastal geomorphic processes currently occurring around the island. Santa Cruz Island is located off Southern California, USA and is partially exposed to open ocean swell from the northwest and south. Wave energy and significant energy dissipation on shorelines correlates with (1) shore orientation relative to the W-NW swell, (2) nearshore bathymetry, and (3) type of shoreline impacted by waves.

Background

Water waves can be described with mathematical approximations. These approximations can handle a variety of conditions, however all methods have limitations. Waveforms are extremely dynamic and behave differently in offshore, transition zone and near-shore environments. Two main classes of wave theory have emerged to describe waves: linear or small amplitude wave theory, and shallow (or non-linear) wave theory.

Linear wave theory was first presented by Airy (1845) to provide methods to calculate wave characteristics like height, period, and speed using a sinusoidal model of the waveform. Airy's model continues to be used due to its ease of use and ability to accurately represent offshore wave conditions. Extensions include calculations for particle velocity, wave energy and energy flux (USACE, 1984). Linear wave theory relies on the assumption of closed circular particle orbits (Figure 8.1). This assumption breaks down in the transition zone approaching shore, where these circular particle orbits interact with the sea floor and cause waveform changes to occur.
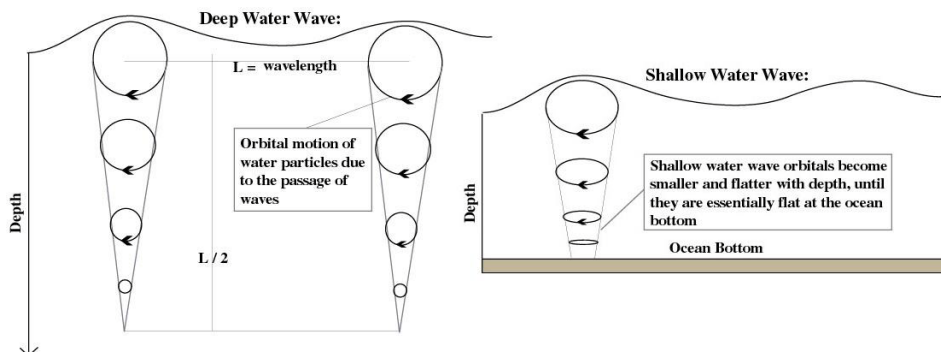

Figure 8.1. Airy's linear theory of wave motion breaks down when waves enter shallow water. Adapted from New South Wales Coastline Management Manual (1990).

Shallow wave theory picks up where linear theory deviates from observation – in the transition zone. Generally, all non-linear analysis techniques are grouped into shallow wave theory. These formulations are more complicated than linear theory, but are necessary to incorporate sea floor slope, viscous wave effects and frictional losses due to wave – sea floor interaction. Properties like mass transport can be estimated (closed circular orbits not required) and pressure and velocity fields more accurately predicted than with linear models (USACE, 1984). Shallow waves are presented in detail in Dean and Darymple (1991) and Svendsen (2006).

This study draws from both theories and several empirical equations to complete an offshore and near-shore analysis of wave activity. Linear theory is used to calculate incoming wave characteristics and give estimates of offshore wave energy and wave energy flux. As waveforms approach shore they deviate from the sinusoidal form and become shallow water waves. Shoaling and refraction and diffraction equations are used to describe these effects on wave height. Lastly, waves break or reflect on the shoreline imparting varying amounts of energy through pressures based on type of contact.

Methods

There are three major zones of wave analysis. The first is offshore characteristics, which is influenced by larger oceanic and atmospheric processes and sets up the nearshore analysis. As waves approach shore they enter a transitional zone and begin to change. A shoaling, refraction, and diffraction (SRD) model is developed from available theory to calculate wave transformations. Lastly, waves move into the dissipation zone and transfer energy as pressure to shorelines. Figure 8.2 presents a schematic of these zones. The following subsections outline each in detail.
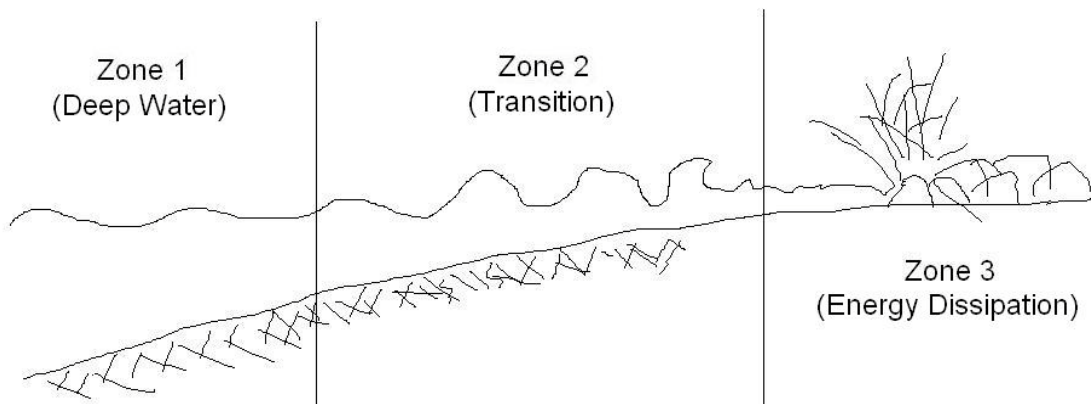

Figure 8.2. Three analysis zones of offshore waves, nearshore transformations, and energy dissipation.

Zone 1: Offshore Calculations

Deep water waves travel without interacting with the sea floor, and can be described fairly accurately with linear theory. These waves are defined by water depths greater than half the wavelength (d >L_0/2). The following equations define offshore wave parameters (subscript 0 means deep water).

$$C_0 = L_0 / T \tag{8.1}$$

$$C_g = 1/2 * C_0 \tag{8.2}$$

$$E = \sigma * g * (H_0)^2 * L_0 / 8 \tag{8.3}$$

$$P = E_{avg} * C_g \tag{8.4}$$

Where C_0 is wave celerity, L_0 is wavelength, T is wave period, C_g is group celerity, E is wave energy, σ is density, g is gravity, H_0 is wave height, P is energy flux and E_{avg} is E / L_0. US ACE Shore Protection Manual (1984) provides derivations and examples.

Zone 2: Transition and Shoaling

As waves approach a shoreline they begin to interact with the sea floor. This frictional process compresses wave particle orbits causing a reduction in wavelength and celerity, and an increase in wave height. This can be thought of as a transfer of wave energy from kinetic to potential.

The shoaling component of the SRD model is based on transitional wave equations (linear & non-linear) and is used to estimate increases in wave height as a function of sea floor slope and incoming wave characteristics. This model is used to predict breaking wave heights and to verify if breaking or reflection occurs at the shoreline. Figure 8.3 is a sample output of the model.
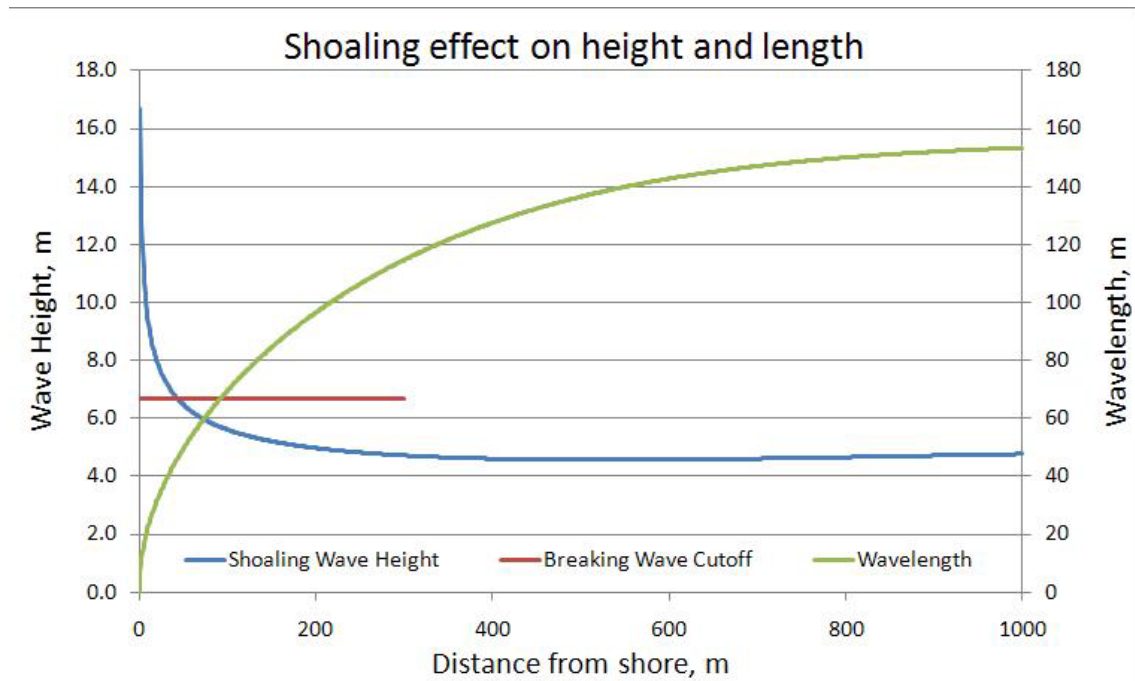

Figure 8.3. Effects of shoaling on incoming wave height and wavelength (H'$_0$ = 4.5m, T = 10 sec).

The SRD model is the basis of the transitional zone analysis. It has inputs for refraction and diffraction (see sections below) and calculates the cumulative effects of these processes on wave height and breaking location. The equations given below are used in the shoaling calculation.

$$L = g * T^2 / (2 * \pi) * [\tanh(4 * \pi^2 * d / (g * T^2))]^{0.5} \qquad (8.5)$$

$$K_S = [0.5 * 1 / n * C_0 / C]^{0.5} \qquad (8.6)$$

$$n = 0.5 * [1 + 4 * \pi * d / (L * \sinh(4 * \pi * d / L))] \qquad (8.7)$$

$$H / H'_0 = K_S * K_R * K' \qquad (8.8)$$

Where L is the refracted wavelength, K_S is the shoaling coefficient, n is the wave number, K_R is the refraction coefficient, and K' is the diffraction ratio. Equation 8.5 is an approximation given by the US ACE SPM (1984) to shortcut the iterative step of finding L based on C or H (functions of L). Equation 8.8 is used to find the adjusted wave height based on the three processes. Breaking wave height is evaluated by $(H / L)_{max} = 1/7$. Steeper waves have crest velocities that exceed average wave celerity and break (Svendsen, 2006).

Calculating the Refraction Coefficient

Refraction is the directional change a wave experiences when it contacts the sea floor and slows down. At a depth of half the wavelength a wave begins to drag along the bottom and its speed is reduced. When this happens locally, the wave appears to turn toward shallow water. Submerged ridges tend to focus wave direction (and increase height, $K_R > 1.0$) while sea floor depressions do the opposite. This process is shown in Figure 8.4. In shallow water, waves refract to follow bathymetry, adjusting to travel perpendicular to lines of equivalent depth on the sea floor.
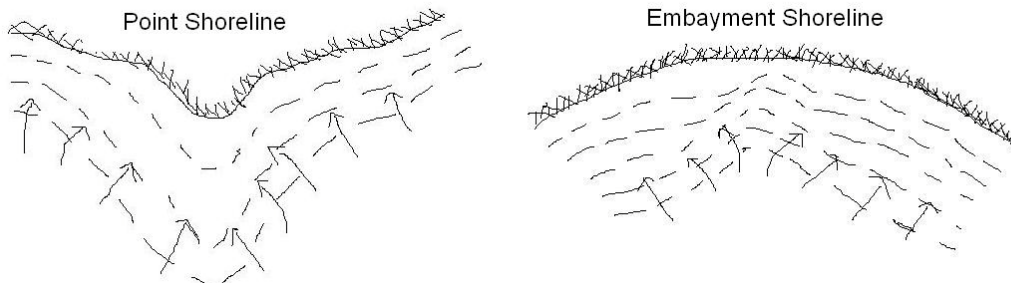

Figure 8.4. Waves approach the shoreline and refract to adjust for an underwater ridge (left), and a sea canyon.

The US ACE SPM (1984) presents time-intensive graphical and numerical approaches that discretize bathymetry contours and apply Snell's Law of general wave refraction (based on wave angle and speed). By assuming parallel contours to the shoreline and constant sea floor slope a simplified refraction coefficient (K_R) can be estimated.

$$\alpha = asin\,[\,C\,/\,C_0 * \sin(\alpha_0)\,] \tag{8.9}$$

$$K_R = [\,\cos(\alpha_0)\,/\,\cos(\alpha)\,] \tag{8.10}$$

Where α is the refracted wave angle (relative to shore), and α_0 is the incident wave angle. Equations 8.9 and 8.10 require two points for refraction analysis: C and C_0. C is calculated at the breaking wave location in the SRD model because energy dissipation rapidly occurs after this point.

Calculating the Diffraction Ratio

Diffraction is the spreading of wave energy behind swell-blocking obstacles. Waves cut off by a point, jetty, or harbor entrance will display this behavior by wrapping around the obstacle. Significant loss in wave height and energy is associated with diffraction. US ACE SPM (1984) present graphical figures for estimating the effects of diffraction. Figure 8.5 shows an aerial photo of diffraction and a graph from US ACE SPM (1984) that gives iso-K' lines. K' is the diffraction ratio (H / H'$_0$).
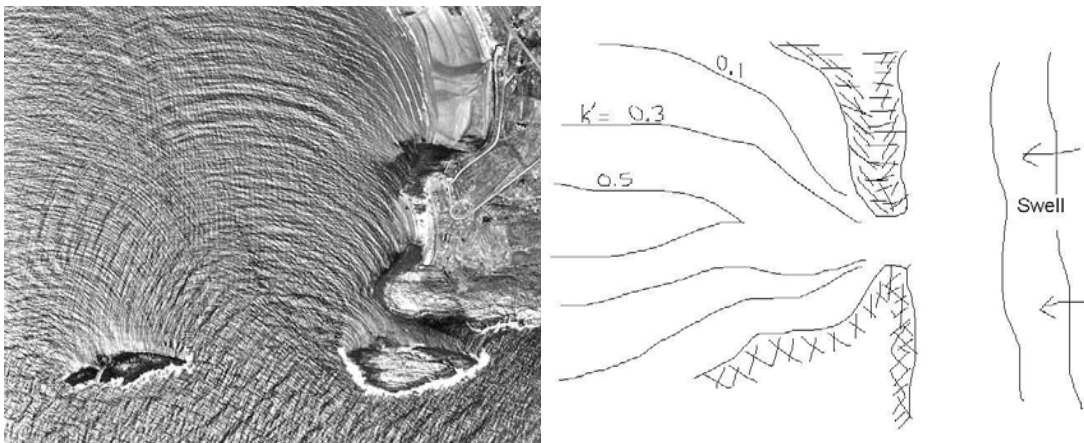

Figure 8.5. Aerial photo of diffraction through an island opening (left) and a sketch of iso-K' lines for diffraction ratio. Photo from ESF Science Wordpress Online. Sketch adapted from USACE SPM (1984).

For this analysis, K' is only estimated at a few locations on the eastern and southeastern sides of Santa Cruz Island. Graphs from US ACE SPM (1984) that best represent the geometry of eastern and southeastern sections are input in the SRD model for calculating wave height.

Zone 3: Energy Dissipation

Bathymetry, Wave-Type and Wave Height

The primary drivers of wave-type are refracted wave height, near-shore bathymetry, and shore topography. Wave-type can be divided into four categories: (1) reflecting waves, (2) spilling breakers, (3) plunging breakers, and (4) surging waves. Gross (1993) diagrams each wave-type in his introductory oceanography book, displayed as Figure 8.6. Each wave-type impacts the shoreline differently and transfers different amounts of total energy as well as peak pressures.
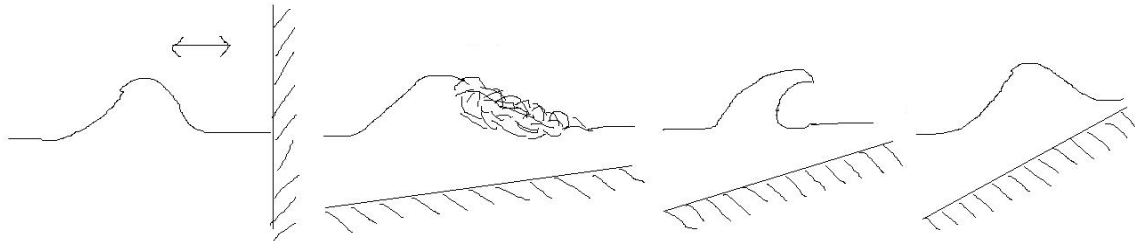

Figure 8.6. Four types of waves from left to right: reflecting waves, spilling breakers, plunging breakers, and surging waves. Each wave type has a unique pressure signature. Adapted from Dean (1991).

In his discussion of wave-types Horikawa (1978) gives the results of pressure impacts on a vertical wall under laboratory conditions. His results are shown in Figure 8.7 for two reflected waves (small and large), a spilling breaker, and a plunging breaker impacting the wall. Breaking waves exert higher pressures over shorter time intervals (and smaller areas – just the surf zone band) than reflecting waves.
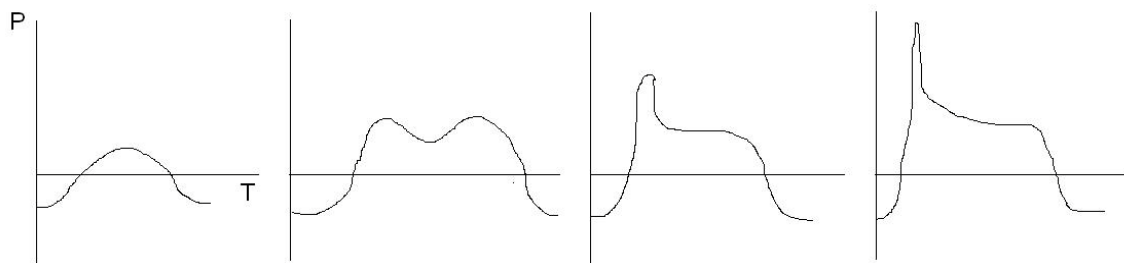

Figure 8.7. Pressure readings for different wave-type impacts. Left to right: small reflecting wave, large reflecting wave, spilling breaker, and plunging breaker. Adapted from Horikawa (1978).

Energy and Pressure Dissipation

Reflected wave pressure is calculated as the combined hydrostatic and dynamic pressure distributions on a cliff face. Horikawa (1978) simplifies Sainflou's formulation by linearizing pressure distributions. Figure 8.8 shows the linear distribution for a crest and trough impacting a cliff face. Pressure oscillations occur in phase with wave period causing a cyclic loading on the cliff face.
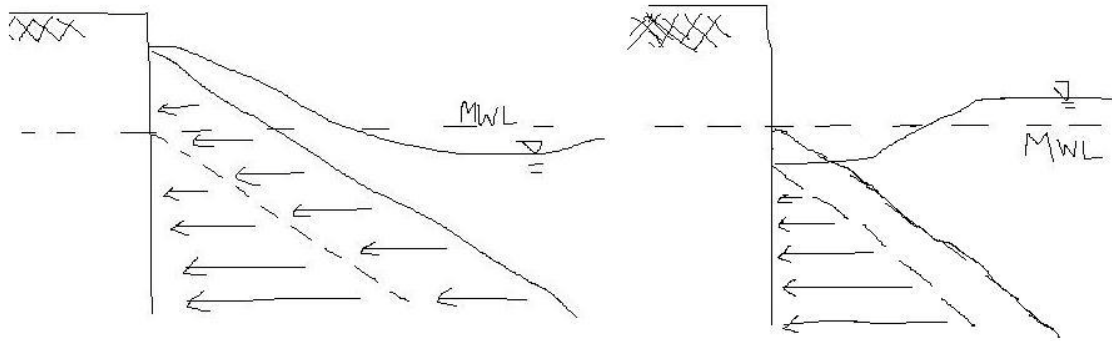
Figure 8.8. Pressure distributions on a vertical cliff face. Hydrostatic is shown as the dotted line and dynamic as the solid line in both figures.

Wave crest (P_C) and trough (P_T) pressures (per unit coastline), assuming simplified hydrostatic and dynamic conditions, are given by the following formulas:

$$P_C = 0.5 * \sigma * g * (d + H_b)^2 \tag{8.11}$$

$$P_T = 0.5 * \sigma * g * (d - H_b)^2 \tag{8.12}$$

Where d is water depth at mean water line (MWL) and H_b is the nearshore wave height. Oscillating pressure distributions are obtained by removing the hydrostatic component.

Breaking waves dissipate more energy on the shoreline than reflected waves. These waves cannot be dealt with analytically, so empirical methods have been developed. To simplify this analysis, all breaking waves are grouped together using the US ACE SPM (1984) formula for general breaking wave impacts:

$$R_m = 0.5 * \sigma * g * (d_b + H_b) * (0.78 * H_b) \tag{8.13}$$

Where R_m is the breaking wave pressure (per unit coastline) and is equal to the hydrostatic pressure of the breaking wave multiplied by an empirical breaking factor (0.78 * H_b), d_b is depth at breaking, and H_b is the breaking wave height. Although this simplification reduces the sensitivity of nearshore interaction down to a single breaking wave impact it still provides a quantitative estimate of the overall impact felt by the shoreline.

Analysis

Pacific Ocean Swells

Primary ocean swell direction near Southern California is dependent on the season. During winter months the west-northwest (W-NW) swell dominates (Figure 8.9A). Rose plots in Xu and Noble (2009) show this swell arriving from 270 to 300 degrees at unsheltered buoys. During the summer months a weaker swell arrives from the south (Figure 8.9B) and impacts the south coast of Santa Cruz Island. Note the transition in primary swell direction and magnitude around Santa Cruz Island due to the seasonal transition from winter to summer. The scope of this analysis is

limited to the study of shoreline impacts due to the W-NW swell and qualitative comments will be made regarding the effects of the southern swell.
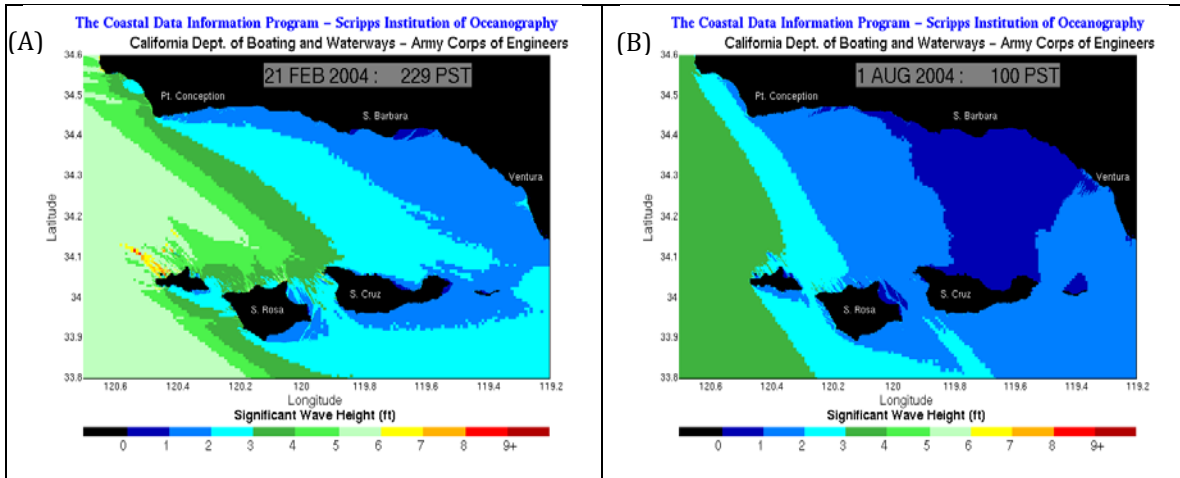

Figure 8.9. Two primary swell directions in the Southern California bight, **[A]** winter swell and **[B]** summer swell.

The W-NW swell is generated by Northern Hemisphere Polar Westerlies (Gross, 1992) and is the stronger of the seasonal swells. Its deep water energy ranges from 372 to 3970 kN per wavelength per meter width. The 95% (storm) wave height for W-NW swell is shown in Figure 8.10. Xu and Noble (2009) characterize Pacific storm events using a cumulative distribution function with a 95% cutoff threshold.

Refraction and Diffraction Analysis

Refraction orthogonals are shown in Figure 8.10. Dividing lines (sections AA and BB) indicate a change in primary swell direction based on remaining swell energy nearshore. The southern part of Santa Cruz Island is sheltered by offshore islands and incurs large reductions in W-NW swell energy by refraction and diffraction processes. The southern swell is hypothesized to become the dominate swell below these section lines in the summer months. This is due to the seasonal weakening of storm generation in the North Pacific as well as increasing generation in the South Pacific (see Figure 8.11).
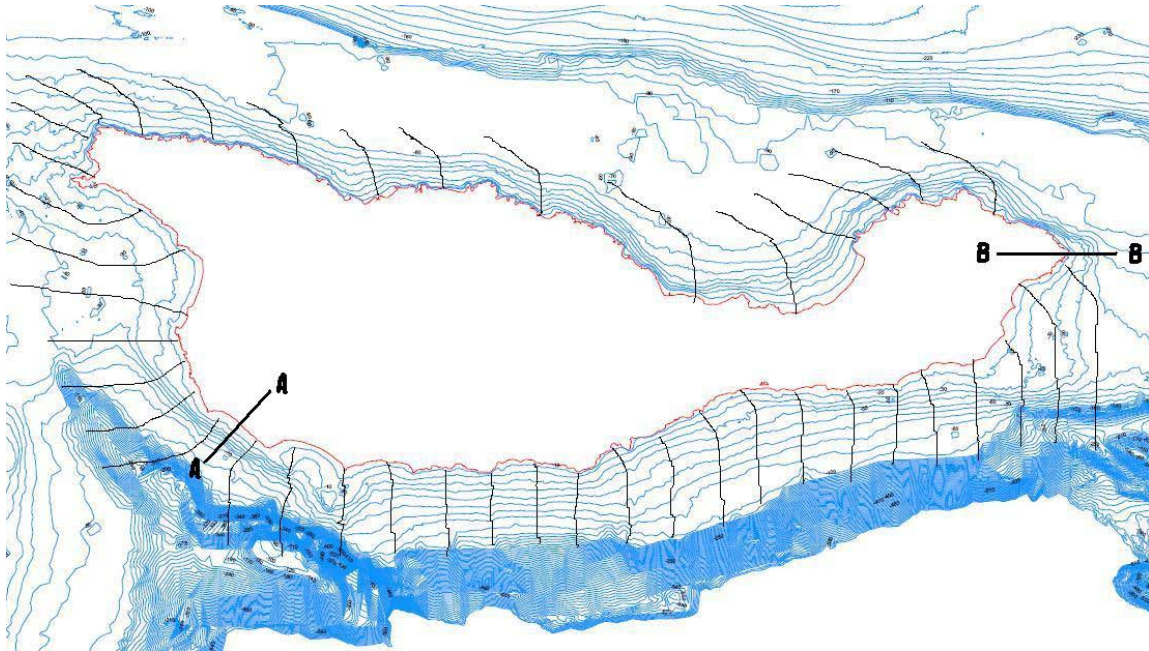
Figure 8.10. Orthogonal rays for maximum yearly wave heights: W-NW winter swell (above AA and BB) and southern summer swell (below AA and BB).
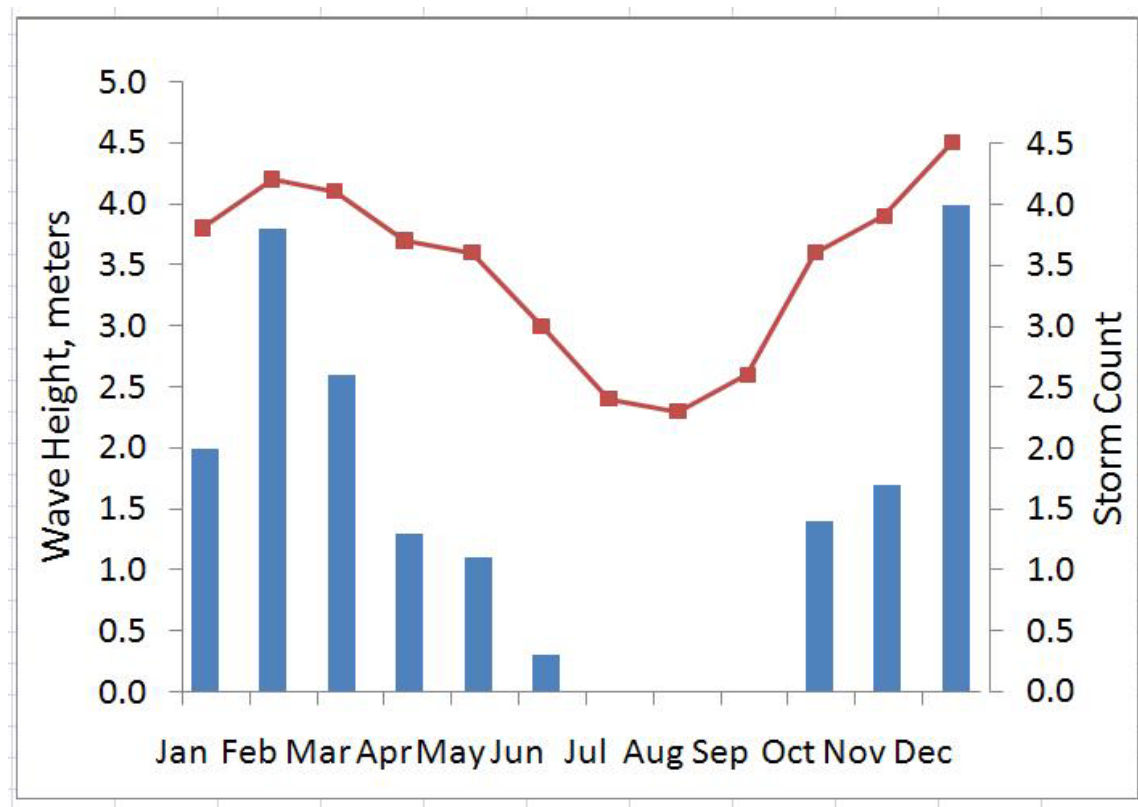

Figure 8.11. Storm wave height (95 percentile) and storm count (blue bars) near Point Conception, CA.

SRD model output is generated for nine cross sections along the Island. Each cross section was chosen because it represents a unique condition, such as north-facing and shallow beach, or west-facing and vertical cliff. Table 8.1 gives input and output variables from the model for two scenarios, W-NW storm conditions in August and storm conditions in December. These two scenarios estimate the range of expected yearly wave energy due to storm swell activity.

Table 8.1. SRD model data for storm conditions in August and December.

Small Waves (August 95% Hs = 2.3 m, T = 6 sec)

Section	H_0	T	α_0	Slope	K_S (at x_b)	K_R (at x_b)	K'	H_b	x_b	d (at x = 0)	Shore Type	Reflect or Break
1	2.3	6	20	0.013	1.25	0.97	1.0	2.79	83	5	Vert Cliff	Reflected
2	2.3	6	80	0.090	1.71	0.42	1.0	1.65	3	7	Vert Cliff	Reflected
3	2.3	6	35	0.040	1.28	0.91	1.0	2.68	24	0	Slope Cliff	Break
4	2.3	6	15	0.030	1.25	0.98	1.0	2.82	36	0	Beach	Break
5	2.3	6	50	0.077	1.34	0.81	1.0	2.50	10	8	Vert Cliff	Reflected
6	2.3	6	50	0.014	3.56	0.80	0.1	0.33	1	0	Beach	Break
7	2.3	6	70	0.043	1.47	0.59	0.5	1.00	12	0	Slope Cliff	Break
8	2.3	6	80	0.024	1.63	0.42	1.0	1.57	14	0	Beach	Break
9	2.3	6	20	0.006	1.25	0.97	1.0	2.79	193	0	Beach	Break

Big Waves (December 95% Hs = 4.5 m, T = 10 sec)

Section	H_0	T	α_0	Slope	K_S (at x_b)	K_R (at x_b)	K'	H_b	x_b	d (at x = 0)	Shore Type	Reflect or Break
1	4.5	10	20	0.014	1.39	0.97	1.0	6.07	131	5	Vert Cliff	Break
2	4.5	10	80	0.059	1.86	0.42	1.0	3.51	9	7	Vert Cliff	Reflected
3	4.5	10	45	0.035	1.45	0.85	1.0	5.54	43	0	Slope Cliff	Break
4	4.5	10	15	0.022	1.38	0.98	1.0	6.12	85	0	Beach	Break
5	4.5	10	55	0.057	1.50	0.76	1.0	5.16	23	8	Vert Cliff	Reflected
6	4.5	10	80	0.011	2.75	0.42	0.3	1.55	10	0	Beach	Break
7	4.5	10	80	0.031	1.82	0.42	0.5	1.71	19	0	Slope Cliff	Break
8	4.5	10	80	0.024	1.83	0.42	1.0	3.44	24	0	Beach	Break
9	4.5	10	15	0.0057	1.38	0.98	1.0	6.12	328	0	Beach	Break

From the model output, breaking wave height (H_b) is larger for December conditions, with waves breaking further offshore (x_b). The implication for cliff faces experiencing reflection pressures is an increase in wave run-up and a corresponding increase in pressure oscillation. For breaking waves, an increase in wave height results in a much larger breaking distance offshore. A simple ratio ($d_{x=0}/H_b <> 1.5$) determines if a wave will be reflected or break.

Energy Impacts: Wave Pressures

The final component of this analysis is to calculate wave pressures impacting the shoreline for each model run. Figure 8.12 shows SRD model cross sections and wave pressures based on the results from Equations 8.11-8.13. Reflected wave pressures are recorded as (+/-) to indicate oscillating wave pressures due to reflection. Table 8.2 provides expanded data for each case. Pressures are given per meter of shoreline width.
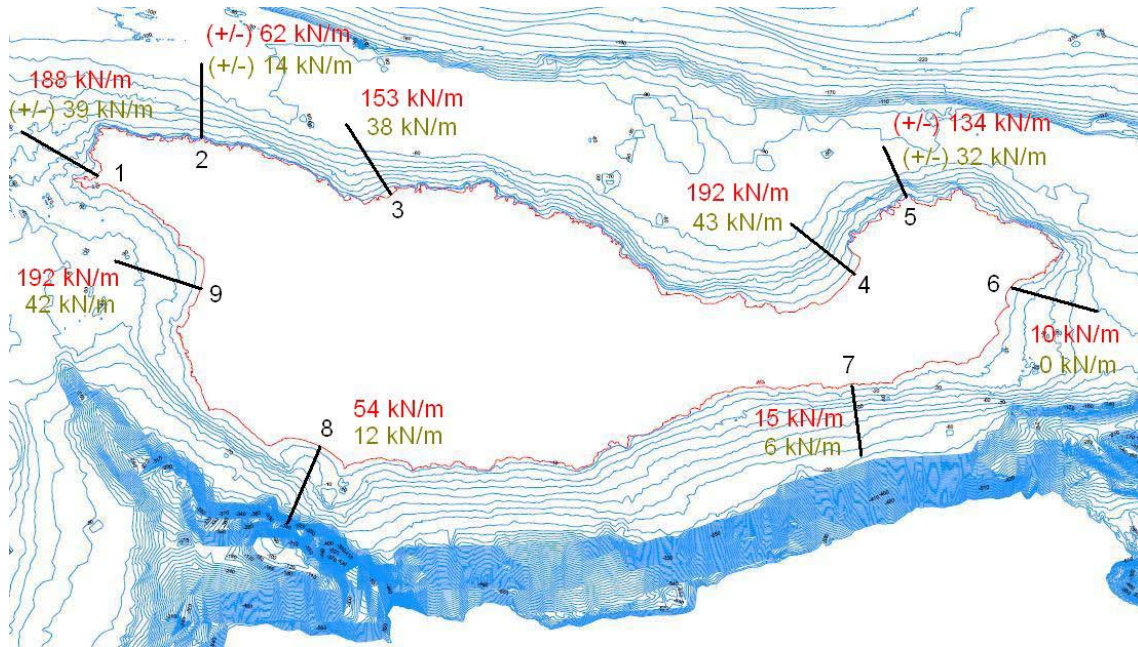
Figure 8.12. SRD model cross-sections and breaking wave pressures. Red indicates December values and green indicates August. Oscillating reflected waves are written with a (+/-) sign.

The difference between pressure impacts under December storm conditions and August storm conditions is striking. Areas experiencing little refraction and diffraction have the largest variability, while sheltered sites on the southern coastline show a dampened response to incoming wave energy.

Table 8.2. Wave impact pressures from reflecting and breaking waves on Santa Cruz Island

Small Waves (August 95% Hs = 2.3 m, T = 6 sec)						Big Waves (December 95% Hs = 4.5 m, T = 10 sec)				
		Reflected Hydrostatic	Reflected Dynamic (+/-)	Breaking Wave Pressure				Reflected Hydrostatic	Reflected Dynamic (+/-)	Breaking Wave Pressure
Section	Shore Type	kN/m	kN/m	kN/m		Section	Shore Type	kN/m	kN/m	kN/m
1	Vert Cliff	126	39			1	Vert Cliff			188
2	Vert Cliff	246	14			2	Vert Cliff	246	62	
3	Slope Cliff			38		3	Slope Cliff			153
4	Beach			43		4	Beach			192
5	Vert Cliff	322	32			5	Vert Cliff	322	134	
6	Beach			0		6	Beach			10
7	Slope Cliff			6		7	Slope Cliff			15
8	Beach			12		8	Beach			54
9	Beach			42		9	Beach			192

Breaking wave pressures are generally higher than reflecting wave pressures due to the limited shoreline contact area of breaking waves and the retaining of kinetic energy for waves reflecting back offshore. High pressures for some westward facing beaches can be misleading. Section 9 for example has a breaking wave pressure of 192 kN/m, but this is applied over the entire breaking zone. A linear (distance from shore) reduction in breaking wave energy is not

physically accurate, but does reduce the shoreline pressure to very small amounts (192kN/m over 328 m).

Lastly, it is expected that with larger conditions a shift from reflecting waves to breaking waves would be observed due to larger waves feeling bathymetry further offshore. Section 1 provides evidence of this effect, the model analysis changes from reflecting to breaking waves based on the reflected wave criterion given above.

Limitations

This paper attempts to conduct an analysis of incoming wave regime and energy impacts along an irregular Island coastline with complex bathymetry. The desire to present meaningful values has resulted in the use of many assumptions and simplifications. These are: (1) only the primary W-NW swell is analyzed in the SRD model, (2) refraction is modeled by constant slope bathymetry orientated parallel to shore and contour lines, and (3) energy dissipation equations are generalized and do not capture irregularities in shorelines.

Withstanding these limitations, an overall description of wave energy and targeted estimates of wave pressures are informative. Limitation (2) will have a variable effect on wave height transformations depending on the shape of the contour lines (see Figure 8.4). Limitation (3) masks the effects of localized intense pressure zones and could have significant implications for shoreline erosion. This limitation cannot be overcome without conducting a more detailed study.

Lastly, energy dissipation on the southern side of the Island is likely to be stronger than the model predicts because the southern swell experiences little refraction and diffraction before impacting the Island. This only occurs in the summer months when the W-NW swell weakens, and experiences reductions due to refraction and diffraction. An estimate of the southern swell impacts can be calculated by using 0.3 to 0.6 m swell conditions (with K_R = 1.0 and K' = 1.0) applied to southern coastline cross sections.

Conclusions

Orientation

The highest energy dissipation rates were found on the NW corner of Santa Cruz Island, indicating the importance of wave direction and the refraction process. Other high dissipation locations exist on adjacent sides of the Island where local shoreline is parallel to incoming swells. Cross sections 4 and 9 are good examples of this effect (generally north-facing and west-facing coastlines respectively).

Locations that are sheltered from primary swell (i.e. the southern and eastern coastlines) experience low impact pressures due to high refraction and offshore sheltering by Santa Rosa Island as well as Santa Cruz itself. Cross section 6 experiences large reductions due to refraction as well as diffraction and makes Scorpion Harbor an ideal place to land boats.

Cliffs and Beaches

Cliffs generally feel less impact because deep water exists in front of them, causing reflecting waves. Reflecting waves only transfer their potential energy to cliffs (hydrostatic plus dynamic loading), and retain kinetic energy as the wave reflects and heads offshore. On the other hand, cliffs can experience the greatest pressure impacts in locations where the bottom is shallow and incoming waves reach breaking height. In these instances most of the wave energy (kinetic and potential) is transferred to the shoreline over a short distance. Cross-section 1 is a good example and has the highest peak pressures of cross-section analyzed once distance of the impact zone is considered. In Chapter 9 we analyze wave energy dissipation in conjunction with rock type and other factors to develop an index of vulnerability for shorelines around the island. Cliffs are of special interest due to their prevalence and wide range of energy dissipation values.

Beaches in this analysis proved difficult to characterize. The methods used do not provide a mechanism to dissipate energy deep in the surf zone and result in high pressures for cross-sections 4 and 9. Overall, the geometry of beaches tends to spread refraction orthogonals, dispersing energy over a wider area and reducing the shoreline impact of waves.

Storm Frequencies

The frequency of large storm events helps determine the rate of energy dissipation along the coastline. Although Chapter 9 looks at relative rates of shoreline response, potential exists for a quantitative assessment. Figure 8.10 shows the number of large storms per month affecting Santa Cruz Island. This data could be combined with the impact of Jan-Dec monthly average storms to determine a yearly rate of high energy events impacting Santa Cruz Island. This approach would be an effective method to compile results from individual event impacts and make predictions regarding the actual response of Santa Cruz Island.

References

Bray, N.A. et al. 1999. "The California Current system in the Southern California Bight and the Santa Barbara Channel." Journal of Geophysical Research 104(C4): 7695-7714

Crapper, G.D. 1984. Introduction to Water Waves. John Wiley and Sons, New York.

Dean, R.G. and Dalrymple, R.A. 1991. Water Wave Mechanics for Engineers and Scientists. World Scientific, London.

Gross, M.G. 1993. Oceanography. Prentice Hall, New Jersey.

Horikawa, K. 1978. Coastal Engineering. University of Tokyo Press, Tokyo.

Sorensen, R.M. 1978. Basic Coastal Engineering. John Wiley and Sons, New York.

Svendsen, I.A. 2006. Introduction to Nearshore Hydrodynamics. World Scientific, London.

US Army Corps of Engineers 1984. Shore Protection Manual I & II. US Government Office of Printing, Washington D.C.

Xu, J.P. and Noble, M.A. 2009. "Variability of the Southern California wave climate and implications for sediment transport." Geological Society of America, Special Paper 454: 171-191